

Similar behaviors between FRB 121102 and solar type III radio bursts

G. Q. ZHANG,¹ F. Y. WANG,^{1,2} AND Z. G. DAI^{1,2}

¹*School of Astronomy and Space Science, Nanjing University, Nanjing 210093, China*

²*Key Laboratory of Modern Astronomy and Astrophysics (Nanjing University), Ministry of Education, Nanjing 210093, China*

ABSTRACT

Fast radio bursts (FRBs) are bright milliseconds radio transients with large dispersion measures (DMs), and can be used as potential astrophysical and cosmological tools. Many models for FRB progenitors have been proposed. However, none of them can explain all the observational properties, meaning that FRBs remain one of the most intriguing mysteries in astronomy. The statistical properties of radio bursts can unveil the underlying physics. Here, we report statistical results of the repeating FRB 121102, and show that FRB 121102 and solar type III radio bursts share four statistical properties: power-law frequency distributions for energies, fluxes, durations and waiting times. All of the distributions can be explained by avalanche models of self-organized criticality (SOC) systems. It is well known that solar type III radio burst arises from the nonlinear conversion of Langmuir waves generated by two-stream instability of electron beams, which are accelerated by bursty magnetic reconnections. The similarities support that repeating FRBs are coherent emissions from magnetic-reconnection-driven beams in the magnetospheres of magnetars.

1. INTRODUCTION

Fast radio bursts (FRBs) are intense radio transients with extreme brightness temperatures that show dispersion relations consistent with propagation through cold plasma (Lorimer et al. 2007; Thornton et al. 2013; Petroff et al. 2016). Until now, more than seventy FRBs have been discovered. Only FRB 121102 and FRB 180814 show repeating bursts (Spitler et al. 2014, 2016; CHIME/FRB Collaboration et al. 2019). The sub-arcsecond localization of FRB 121102 using the VLA confirmed its cosmological origin (at redshift 0.193) (Chatterjee et al. 2017). The combined redshift and DM information of FRBs can be used as cosmological probes if a large sample of FRBs has redshift measurements (Deng & Zhang 2014; Gao et al. 2014; McQuinn 2014; Zheng et al. 2014; Zhou et al. 2014; Wei et al. 2015; Yu & Wang 2017; Macquart 2018; Li et al. 2018; Wang, & Wang 2018; Walters et al. 2018). However, the physical origin of FRBs is still mystery (Pen 2018). There are many models have been proposed (Totani 2013; Falcke & Rezzolla 2014; Zhang 2014; Cordes & Wasserman 2016; Dai et al. 2016; Wang et al. 2016; Zhang 2016; Katz 2016; Metzger et al. 2017; Zhang 2017; Pen 2018; Platts et al. 2018). On the other hand, it is well known

that solar type III radio bursts, identified by high brightness temperatures and rapid frequency drift, are a common signature of fast electron beams in the solar corona (Bastian et al. 1998). It arises from the nonlinear conversion of Langmuir waves generated by two-stream instability of electron beams (Ginzburg, & Zhelezniakov 1958; Melrose 2017; Kliem et al. 2000). There are at least three common properties for repeating FRBs and solar type III radio bursts. First, they both have high brightness temperatures, 10^6 K- 10^{12} K for solar radio bursts and as high as 10^{35} K for FRBs. Second, the frequency drift (high-to-low temporal evolution) is found in repeating FRB 121102 (Hessels et al. 2018) and FRB 180814 (CHIME/FRB Collaboration et al. 2019), and solar type III radio bursts (Bastian et al. 1998). Third, both radio bursts show similar intensity temporal evolution (CHIME/FRB Collaboration et al. 2019; Hessels et al. 2018; Fainberg & Stone 1974).

Although radio bursts are common phenomena in repeating FRBs and the Sun, the burst energy spans more than 15 orders of magnitude and an outstanding question appears, namely, do repeating FRBs and solar type III radio bursts have a similar physical mechanism? Interestingly, some theoretical models have suggested that repeating FRBs could be magnetically dominated explosive events (Lu & Kumar 2018; Lyutikov 2019), similar as that of solar type III radio bursts. However, a physical analogy between FRBs and solar type III radio bursts has not yet been established. In this paper,

we will investigate the physical connection between the FRB 121102 and solar type III radio bursts.

2. DATA AND METHOD

We collect the bursts of FRB 121102 from the observation by Green Bank telescope at 4-8 GHz. Recent work identified 93 pulses of FRB 121102 from 6 hours of observation (Gajjar et al. 2018; Zhang et al. 2018). This observation constructs the largest sample of FRB 121102 for a single observation. Using this sample, we can avoid the complex selection effect caused by the different telescopes at different frequencies.

As for solar type III radio bursts, we select the data from the National Centers for Environmental Information (NCEI) observed by United States Air Force Radio Solar Telescope Network (RSTN)¹, which has observed for many years and has accumulated lots of data. RSTN consists of four sites: Learmonth, Palehua, Sagamore Hill and San Vito. The device and analysis methods in all sites are identical, so we can simply put them together to study their statistical properties. The data of RSTN contains solar radio bursts at 8 frequencies (245 MHz, 410 MHz, 610 MHz, 1415 MHz, 2695 MHz, 4995 MHz, 8800 MHz, 15400 MHz). We divide the data into multiple subsamples based on frequency and calculate their statistical nature on each frequency. In order to obtain high quality data, we filter the data according to criteria given by Giersch et al. (2017). Based on these criteria, we select a large sample of solar type III radio bursts. The number of bursts in each frequency is listed in Table 1.

The number of bursts of FRB 121102 is small, so it's preferable to consider cumulative distribution rather than differential distribution. We derive the distribution of energy, peak flux and duration time from FRB 121102 and show the results in right panels of Figure 1, Figure 2 and Figure 3. The energy is calculated from $E = 4\pi d_L^2 S \Delta\nu / (1+z)$, where d_L is the luminosity distance, S is fluence, z is redshift and $\Delta\nu$ is bandwidth. It should be noted that we must consider the deviation from ideal power-law distribution. There are many effects that cause this deviation, such as the threshold of telescope and a physical threshold of an instability. Thus we adopt threshold power-law distribution to fit the cumulative distribution, which is

$$N(> E) = a + b(E^{1-\alpha_E} - E_{\max}^{1-\alpha_E}), \quad (1)$$

¹ <ftp://ftp.ngdc.noaa.gov/STP/space-weather/solar-data/solar-features/solar-radio/radio-bursts/reports/fix-frequency-listings/>

where E_{\max} is the maximum energy of FRB and α_E is the power-law index of differential distribution of energy.

We also consider the waiting time of FRB 121102. Taking the difference between the start times of 2 bursts as the waiting time, we compute the differential distribution of waiting time and show it in right panel of Figure 4 as blue points. Below, we use Poisson process to explain the waiting time distributions. For constant burst rate, the waiting time follows the Poisson interval distribution (Wheatland et al. 1998)

$$P(\Delta t) = \lambda e^{-\lambda \Delta t}, \quad (2)$$

where λ is the burst rate. If the rate is time dependent, the distribution can be treated as a piecewise constant Poisson process consisting N intervals with λ_i and duration t_i . The wait time distribution can be derived by Aschwanden (2011)

$$P(\Delta t) \simeq \frac{1}{\bar{\lambda}} \sum_{i=1}^N \frac{t_i}{T} \lambda_i^2 e^{-\lambda_i \Delta t}, \quad (3)$$

where $\bar{\lambda}$ is the average burst rate and T is the duration of the observing period (Wheatland et al. 1998). Equation (3) can be transformed into a continuous function

$$P(\Delta t) = \frac{\int_0^T \lambda(t)^2 e^{-\lambda(t)\Delta t} dt}{\int_0^T \lambda(t) dt}. \quad (4)$$

In this case, we adopt an exponentially growing occurrence rate (Aschwanden 2011), and obtain $P(\Delta t) = \lambda_0 / (1 + \lambda_0 \Delta t)^2$. Using the Markov chain Monte Carlo (MCMC) method, we derive $\lambda_0 = 1.23_{-0.38}^{+0.80} \times 10^{-5} \text{ ms}^{-1}$.

The differential distributions of energy, peak flux, duration and waiting time for solar type III radio bursts are also derived. Unlike FRB 121102, the number of solar radio bursts is large enough to get a differential distribution. The data of RSTN consists with eight frequencies. In these frequencies, 4995 MHz is more interested, because it has the similar frequency with the data of FRB 121102. We use ideal power-law function to fit the differential distributions of energy, peak flux and duration. This function form is

$$dN/dE \propto E^{-\alpha_E}, \quad (5)$$

where α_E is the power-law index. Assuming the number of solar radio bursts in a given bin satisfies Poisson distribution, the best-fitting results are derived using MCMC methods. The power-law index of energy is 1.63 ± 0.06 , the power-law index of peak flux is 1.84 ± 0.04 and the power-law index of duration is 1.69 ± 0.02 . The fitting results show in left panels of Figure 1, Figure 2 and Figure 3. As for waiting times,

the differential distribution is derived. We still use $P(\Delta t) = \lambda_0/(1 + \lambda_0\Delta t)^2$ to fit the distributions. As for the solar radio bursts in other seven frequencies, we also derive the distributions and fit these distributions with the same function. We give the best-fitting values for α_E , α_F , α_T and λ_0 in Table 1. The best-fitting values are consistent with each other for the eight frequencies.

3. RESULTS

In this paper, we compare statistical properties of the energy, flux, duration and waiting time distributions. We collect 21 bursts (Gajjar et al. 2018) and 72 bursts (Zhang et al. 2018) of FRB 121102 recorded with the C-band receiver at the Green Bank Telescope (GBT). Due to the small number of bursts, the cumulative distribution is performed. The energy distribution shows a flat part at the low-energy regime, which could be due to incomplete sampling and some selection bias for large bursts (Aschwanden 2015). Therefore, in order to avoid the selection effect, only the distribution above the break is fitted. The right panel of Figure 1 shows the energy cumulative distribution of FRB 121102. The red line is best-fitting with $\alpha_E = 1.63 \pm 0.06$, which consistent with the value found by Wang, & Yu (2017) and Law et al. (2017).

For solar type III radio bursts, The energy of solar type III radio bursts can be derived from $E = 4\pi D^2 S \Delta\nu$, where $D = 1$ AU, $S \simeq T \times F$, and $\Delta\nu = 14$ MHz is the bandwidth. T is the duration time and F is the flux of radio bursts. We derive the differential distribution of energy at 4995 MHz, which is closest to the frequency of FRB data. From equation (5), the power-law index of energy is $\alpha_E = 1.52 \pm 0.05$, which is shown as red line in left panel of Figure 1. It must be noted that similar indices are found at different frequencies (see Table 1). The value of α_E is consistent with those previous works (Saint-Hilaire et al. 2013). From Figure 1, similar distributions of energy are found between FRB 121102 and solar type III radio bursts.

Figure 2 shows the differential distribution of peak flux F for solar type III radio bursts at 4995 MHz (left panel) and the cumulative distribution of peak flux for FRB 121102 (right panel), respectively. Using the same fitting method as Figure 1, we find the power-law indices are $\alpha_F = 1.84 \pm 0.04$ and $\alpha_F = 1.94 \pm 0.03$ for solar radio bursts and FRB 121102, respectively. Solar type III radio bursts at different frequencies show similar distributions (see Table 1). The value of α_F for FRBs is consistent with that found by Wang, & Yu (2017).

Figure 3 shows the differential distribution of duration T for solar type III radio bursts at 4995 MHz (left panel) and the cumulative distribution of duration for

FRB 121102 (right panel), respectively. Using the same fitting method as Figure 1, we find the power-law indices are $\alpha_T = 1.69 \pm 0.02$ and $\alpha_T = 1.57 \pm 0.13$ for solar radio bursts and FRB 121102, respectively. Solar type III radio bursts at different frequencies show similar distributions (see Table 1).

From Figures 1, 2 and 3, we have found a similar power-law dependence of the occurrence rate for both radio bursts, very similar to what is found in solar flares (Crosby et al. 1993; Aschwanden 2011; Wang & Dai 2013). These three properties are predicated by avalanche models of self-organized criticality (SOC) systems (Bak et al. 1988, 1987; Lu & Hamilton 1991). For example, from numerical simulations, Lu & Hamilton (1991) have found that the power-law indices of solar flares are $\alpha_E \sim 1.5$, $\alpha_F \sim 1.8$ and $\alpha_T \sim 1.6$ for energy, peak flux and duration distributions, respectively. Therefore, both radio bursts are SOC events. The concept of SOC was proposed to explain the power-law and scale-invariant correlations extending many orders of magnitude in complex systems (Bak et al. 1988, 1987). SOC governs many nonlinear dissipative systems of our universe (Aschwanden 2011).

What can we learn from the similar distributions between solar type III radio bursts and FRBs? It is generally believed that type III bursts arise from the nonlinear conversion of Langmuir waves at the local plasma frequency by energetic electron beams accelerated during solar flares (Ginzburg, & Zhelezniakov 1958; Robinson & Cairns 2000). Numerical simulations have revealed that solar radio bursts are caused by particle acceleration episodes that result from bursty magnetic reconnection (Kliem et al. 2000). From observations, direct evidences have been found that energetic electrons are accelerated by magnetic reconnections, which also produce X-ray flares (Cairns et al. 2018). So type III radio bursts are triggered by magnetic reconnections. As for FRB 121102, the radio emission may be coherent radiation by bunches of relativistic electrons that result from magnetic reconnection in the magnetosphere of a magnetar (Katz 2016; Metzger et al. 2017; Lu & Kumar 2018; Lyutikov 2019). The similar flux and duration distributions support that both radio bursts are triggered by magnetic reconnection.

The fourth statistical property is the waiting time distribution, which has been studied in solar X-ray flares (Wheatland et al. 1998), and X-ray flares in black hole systems (Wang & Dai 2013; Wang et al. 2015). The waiting time Δt is defined as the time interval between two successive bursts. This distribution provides extra constraints on theoretical models. For example, avalanche models predict that bursts occur indepen-

dently (Aschwanden 2011; Lu et al. 1993). Figure 4 shows the occurrence rates as a function of waiting times for solar type III radio bursts at 4995 MHz (left panel) and FRB 121102 (right panel), respectively. A Poissonian random process has a power-law-like waiting time distribution for a time-dependent rate, which is the prediction of the SOC theory (Aschwanden 2011). We fit the waiting time distribution with

$$P(\Delta t) = \frac{\lambda_0}{(1 + \lambda_0 \Delta t)^2}. \quad (6)$$

For large waiting times ($\Delta t \gg 1/\lambda_0$), it gives the power-law limit $P(\Delta t) \approx \Delta t^{-2}$. The fitting results from MCMC method using equation (6) are shown as solid lines in Figure 4. The mean rates are $\lambda_0 = 1.23_{-0.38}^{+0.80} \times 10^{-5} \text{ ms}^{-1}$ for FRB 121102 and $1.10_{-0.01}^{+0.11} \times 10^{-5} (6s)^{-1}$ for solar radio bursts. The waiting times at other frequencies can be also well fitted using equation (6) (see Table 1).

4. DISCUSSION

In this paper, we find that repeating FRB 121102 and solar type III radio bursts have similar statistical prop-

erties, which are predicted by SOC systems. The similarities, together with the type III radio bursts are triggered by magnetic reconnection, indicate that repeating FRBs are powered by magnetic energy within magnetars magnetospheres. Many facilities join the FRB searches, such as Parkes (Petroff et al. 2016), the Australian Square Kilometer Array Pathfinder (ASKAP) (Johnston et al. 2009), UTMOST (Bailes et al. 2017), the Canadian Hydrogen Intensity Mapping Experiment (CHIME) (CHIME/FRB Collaboration et al. 2019), the Five-hundred-meter Aperture Spherical radio Telescope (FAST) (Li et al. 2018), and MeerKAT (Sanidas et al. 2018). In future, large sample of FRBs may unveil underlying physics.

We would like to acknowledge the National Centers for Environmental Information (NCEI) and their past and present staff who work to make space weather data freely available. We also thank X. Cheng and Y. C. Zou for discussions. This work is supported by the National Natural Science Foundation of China (grant No. U1831207, 11573014 and 11833003) and the National Key Research and Development Program of China (grant No. 2017YFA0402600).

REFERENCES

- Aschwanden, M. J. 2011, *Self-Organized Criticality in Astrophysics*.
- Aschwanden, M. J. 2015, *ApJ*, 814, 19
- Bailes, M., Jameson, A., Flynn, C., et al. 2017, *PASA*, 34, e045.
- Bak, P., Tang, C., & Wiesenfeld, K. 1987, *PhRvL*, 59, 381.
- Bak, P., Tang, C., & Wiesenfeld, K. 1988, *Physical Review A*, 38, 364.
- Bastian, T. S., Benz, A. O., & Gary, D. E. 1998, *ARA&A*, 36, 131.
- Cairns, I. H., Lobzin, V. V., Donea, A., et al. 2018, *Scientific Reports*, 8, 1676.
- Chatterjee, S., Law, C. J., Wharton, R. S., et al. 2017, *Nature*, 541, 58.
- CHIME/FRB Collaboration, Amiri, M., Bandura, K., et al. 2019, *Nature*, 566, 235.
- Cordes, J. M., & Wasserman, I. 2016, *MNRAS*, 457, 232.
- Crosby, N. B., Aschwanden, M. J., & Dennis, B. R. 1993, *SoPh*, 143, 275.
- Dai, Z. G., Wang, J. S., Wu, X. F., et al. 2016, *ApJ*, 829, 27.
- Deng, W., & Zhang, B. 2014, *ApJ*, 783, L35.
- Fainberg, J., & Stone, R. G. 1974, *SSRv*, 16, 145.
- Falcke, H., & Rezzolla, L. 2014, *A&A*, 562, A137.
- Gajjar, V., Siemion, A. P. V., Price, D. C., et al. 2018, *ApJ*, 863, 2.
- Gao, H., Li, Z., & Zhang, B. 2014, *ApJ*, 788, 189.
- Giersch, O. D., Kennewell, J., & Lynch, M. 2017, *Space Weather*, 15, 1511.
- Ginzburg, V. L., & Zhelezniakov, V. V. 1958, *Soviet Ast.*, 2, 653.
- Hessels, J. W. T., Spitler, L. G., Seymour, A. D., et al. 2018, *arXiv:1811.10748*.
- Johnston, S., Feain, I. J., & Gupta, N. 2009, *The Low-frequency Radio Universe*, 446.
- Katz, J. I. 2016, *ApJ*, 826, 226.
- Kliem, B., Karlický, M., & Benz, A. O. 2000, *A&A*, 360, 715.
- Law, C. J., Abruzzo, M. W., Bassa, C. G., et al. 2017, *ApJ*, 850, 76.
- Li, Z.-X., Gao, H., Ding, X.-H., et al. 2018, *Nature Communications*, 9, 3833.
- Li, D., Wang, P., Qian, L., et al. 2018, *IEEE Microwave Magazine*, 19, 112.
- Lorimer, D. R., Bailes, M., McLaughlin, M. A., et al. 2007, *Science*, 318, 777.
- Lu, E. T., & Hamilton, R. J. 1991, *ApJ*, 380, L89.

- Lu, E. T., Hamilton, R. J., McTiernan, J. M., et al. 1993, *ApJ*, 412, 841.
- Lu, W., & Kumar, P. 2018, *MNRAS*, 477, 2470.
- Lyutikov, M. 2019, arXiv e-prints, arXiv:1901.03260.
- Macquart, J.-P. 2018, *Nature Astronomy*, 2, 836.
- McQuinn, M. 2014, *ApJ*, 780, L33.
- Melrose, D. B. 2017, *Reviews of Modern Plasma Physics*, 1, 5.
- Metzger, B. D., Berger, E., & Margalit, B. 2017, *ApJ*, 841, 14.
- Pen, U.-L. 2018, *Nature Astronomy*, 2, 842.
- Petroff, E., Barr, E. D., Jameson, A., et al. 2016, *PASA*, 33, e045.
- Platts, E., Weltman, A., Walters, A., et al. 2018, arXiv:1810.05836.
- Robinson, P. A., & Cairns, I. H. 2000, Washington DC American Geophysical Union Geophysical Monograph Series, 119, 37.
- Saint-Hilaire, P., Vilmer, N., & Kerdraon, A. 2013, *ApJ*, 762, 60.
- Spitler, L. G., Cordes, J. M., Hessels, J. W. T., et al. 2014, *ApJ*, 790, 101.
- Spitler, L. G., Scholz, P., Hessels, J. W. T., et al. 2016, *Nature*, 531, 202.
- Sanidas, S., Caleb, M., Driessen, L., et al. 2018, *Pulsar Astrophysics the Next Fifty Years*, 406.
- Thornton, D., Stappers, B., Bailes, M., et al. 2013, *Science*, 341, 53.
- Totani, T. 2013, *PASJ*, 65, L12.
- Walters, A., Weltman, A., Gaensler, B. M., et al. 2018, *ApJ*, 856, 65.
- Wang, F. Y., & Dai, Z. G. 2013, *Nature Physics*, 9, 465.
- Wang, F. Y., Dai, Z. G., Yi, S. X., et al. 2015, *ApJS*, 216, 8.
- Wang, J.-S., Yang, Y.-P., Wu, X.-F., et al. 2016, *ApJ*, 822, L7.
- Wang, F. Y., & Yu, H. 2017, *JCAP*, 2017, 23.
- Wang, Y. K., & Wang, F. Y. 2018, *A&A*, 614, A50.
- Wei, J.-J., Gao, H., Wu, X.-F., et al. 2015, *PhRvL*, 115, 261101.
- Wheatland, M. S., Sturrock, P. A., & McTiernan, J. M. 1998, *ApJ*, 509, 448.
- Yu, H., & Wang, F. Y. 2017, *A&A*, 606, A3.
- Zhang, B. 2014, *ApJ*, 780, L21.
- Zhang, B. 2016, *ApJ*, 827, L31.
- Zhang, B. 2017, *ApJ*, 836, L32.
- Zhang, Y. G., Gajjar, V., Foster, G., et al. 2018, *ApJ*, 866, 149.
- Zheng, Z., Ofek, E. O., Kulkarni, S. R., et al. 2014, *ApJ*, 797, 71.
- Zhou, B., Li, X., Wang, T., et al. 2014, *PhRvD*, 89, 107303.

Table 1. The fitting results for solar type III radio bursts at different frequencies.

frequency (MHz)	number of bursts	α_E	α_T	α_F	$\lambda_0(\times 10^{-5}(6s)^{-1})$
245	15150	1.51 ± 0.20	1.80 ± 0.01	1.85 ± 0.01	$6.13^{+0.19}_{-0.18}$
410	4905	1.51 ± 0.19	1.76 ± 0.02	1.81 ± 0.02	$2.64^{+0.21}_{-0.19}$
610	2672	1.51 ± 0.20	1.73 ± 0.03	1.79 ± 0.03	$1.60^{+0.19}_{-0.17}$
1415	1553	1.55 ± 0.19	1.72 ± 0.03	1.83 ± 0.04	$0.66^{+0.08}_{-0.07}$
2695	1625	1.55 ± 0.19	1.71 ± 0.03	1.91 ± 0.04	$0.76^{+0.08}_{-0.07}$
4995	2091	1.52 ± 0.05	1.69 ± 0.02	1.84 ± 0.04	$1.10^{+0.11}_{-0.01}$
8800	2448	1.51 ± 0.19	1.71 ± 0.02	1.78 ± 0.03	$1.42^{+0.12}_{-0.11}$
15400	2044	1.51 ± 0.19	1.72 ± 0.02	1.70 ± 0.03	$1.43^{+0.14}_{-0.13}$

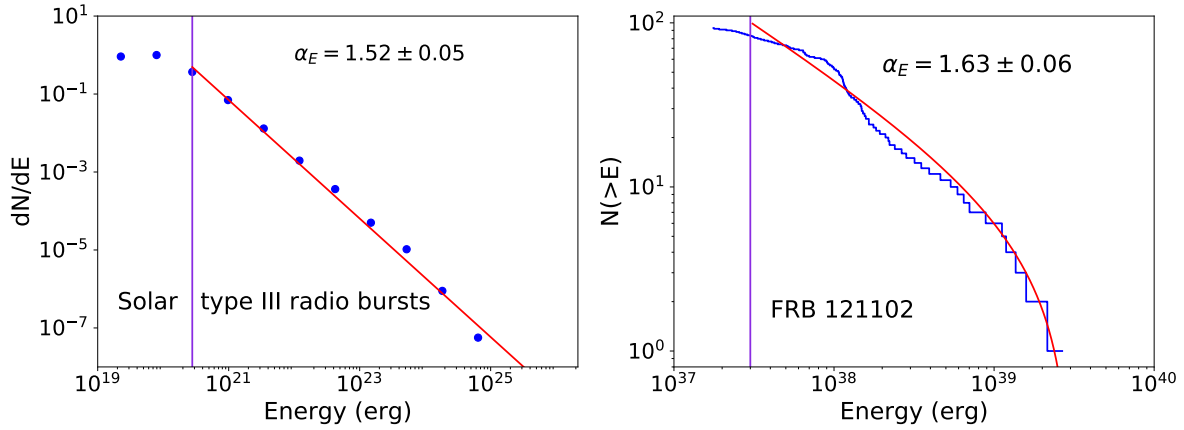


Figure 1. The frequency distribution of Energy. Left panel: the differential distribution of energy for solar type III radio bursts is shown as blue points. The data is observed by the United States Air Force Radio Solar Telescope Network (RSTN) from the National Centers for Environmental information (NCEI) between 1979 and 2010. The best-fitting is shown as red line with power-law index $\alpha_E = 1.52 \pm 0.04$. Right panel: The step-wise blue curve represents the cumulative distribution of energy for FRB 121102. We fit the cumulative distribution using the threshold power-law function $N(> E) = a + b[E^{1-\alpha_E} - E_{\max}^{1-\alpha_E}]$ with $\alpha_E = 1.63 \pm 0.06$, which is shown as red line.

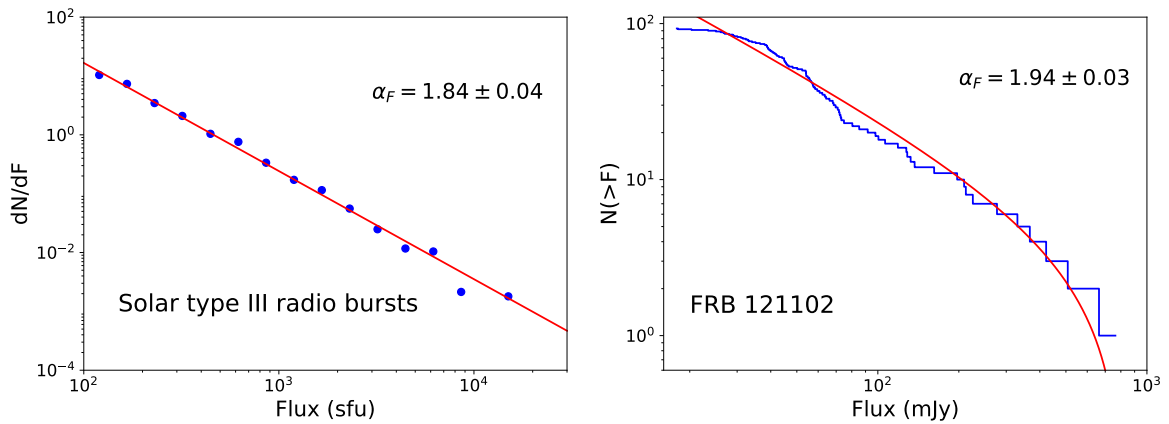


Figure 2. The frequency distribution of peak flux. Left panel: the differential distribution of flux for solar type III radio bursts is shown as blue points ($1 \text{ sfu} = 10^{-22} \text{ W m}^{-2} \text{ Hz}^{-1}$). The best-fitting is shown as red line with power-law index $\alpha_F = 1.84 \pm 0.04$. Right panel: The step-wise blue curve represents the cumulative distribution of flux for FRB 121102. We fit the cumulative distribution using the threshold power-law function $N(> F) = a + b[F^{1-\alpha_F} - F_{\max}^{1-\alpha_F}]$ with $\alpha_F = 1.94 \pm 0.03$, which is shown as red line.

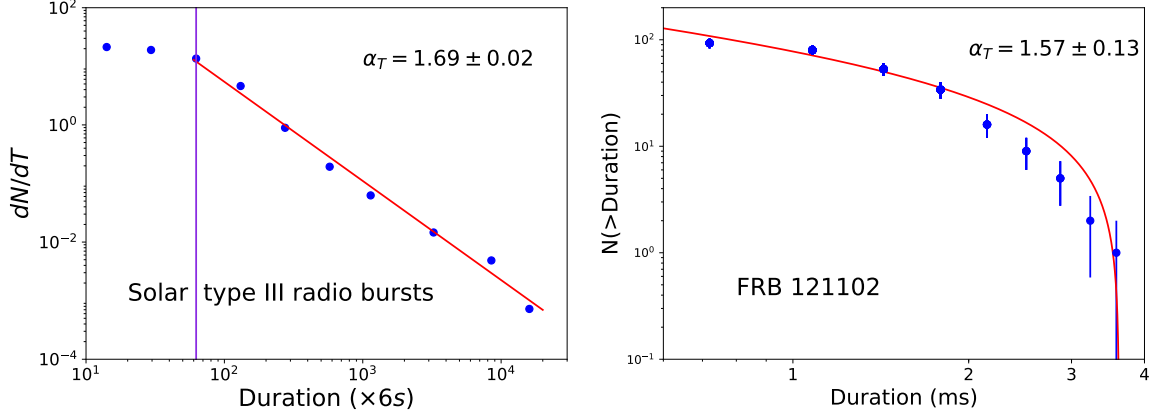


Figure 3. The frequency distribution of burst duration time. Left panel: we give the differential distribution of duration time of solar type III radio bursts blue points. The flat part at the low-duration may be caused by incomplete sampling or other selection effects. Using equation (1) to fit the points above break point, we get the best fitting is $\alpha_T = 1.69 \pm 0.02$. Right panel: The cumulative distribution of duration time of FRB 121102 is shown as blue points. The threshold power-law function $N(> T) = a + b[T^{1-\alpha_T} - T_{\max}^{1-\alpha_T}]$ is used fit this distribution. The best fitting is $\alpha_T = 1.57 \pm 0.13$ (red line).

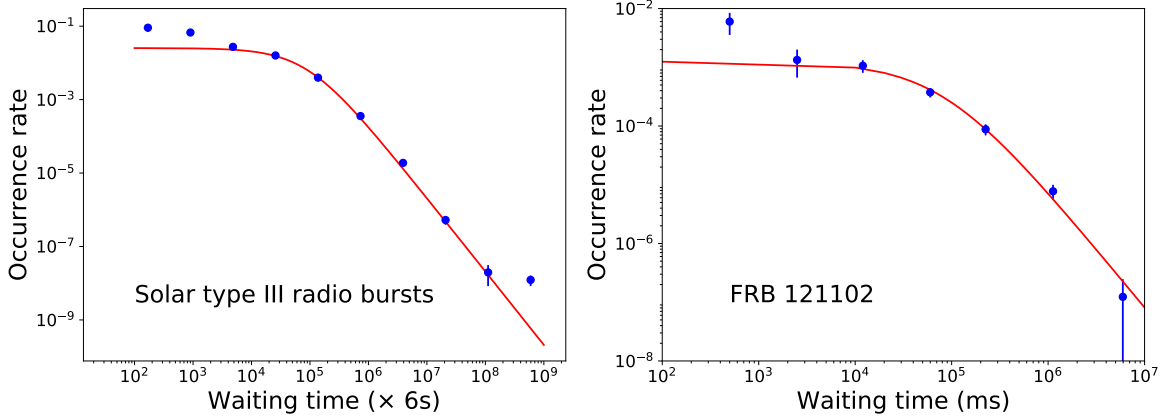


Figure 4. Waiting-time frequency distribution. Considering Poisson random process, we use $P(\Delta t) = \lambda_0 / (1 + \lambda_0 \Delta t)^2$ to fit the distributions. Left panel: occurrence rate as a function of waiting time for solar type III radio bursts is shown as red line with best-fitting parameter $\lambda_0 = 1.10^{+0.11}_{-0.01} \times 10^{-5} (6s)^{-1}$. Right panel: The relation between the occurrence rate and waiting time for FRB 121102. The best-fit power-law index is $\lambda_0 = 1.23^{+0.80}_{-0.38} \times 10^{-5} ms^{-1}$.